

1 **Supplementary information**

2  
3 **Cloud response to co-condensation of water and organic vapors over the boreal**  
4 **forest**

5  
6 Liine Heikkinen<sup>1,2</sup>, Daniel G. Partridge<sup>3</sup>, Wei Huang<sup>4</sup>, Sara Blichner<sup>1,2</sup>, Rahul Ranjan<sup>1,2</sup>,  
7 Emanuele Tovazzi<sup>3</sup>, Tuukka Petäjä<sup>4</sup>, Claudia Mohr<sup>1,2</sup>, and Ilona Riipinen<sup>1,2</sup>

8 <sup>1</sup>Department of Environmental Science (ACES), Stockholm University, Stockholm, Sweden

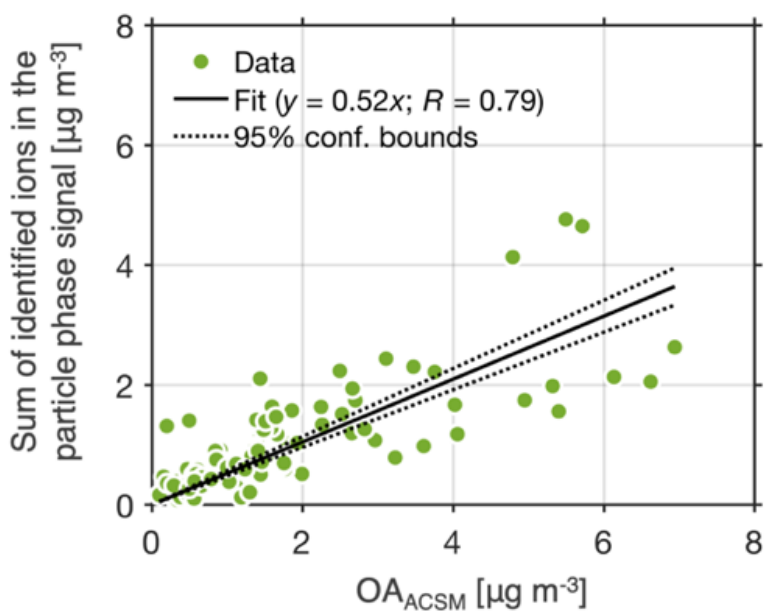
9 <sup>2</sup>Bolin Centre for Climate Research, Stockholm University, Stockholm, Sweden

10 <sup>3</sup>Department of Mathematics and Statistics, Faculty of Environment, Science and Economy, University of Exeter,  
11 Exeter, United Kingdom

12 <sup>4</sup>Institute for Atmospheric and Earth System Research (INAR) / Physics, University of Helsinki, Helsinki, Finland

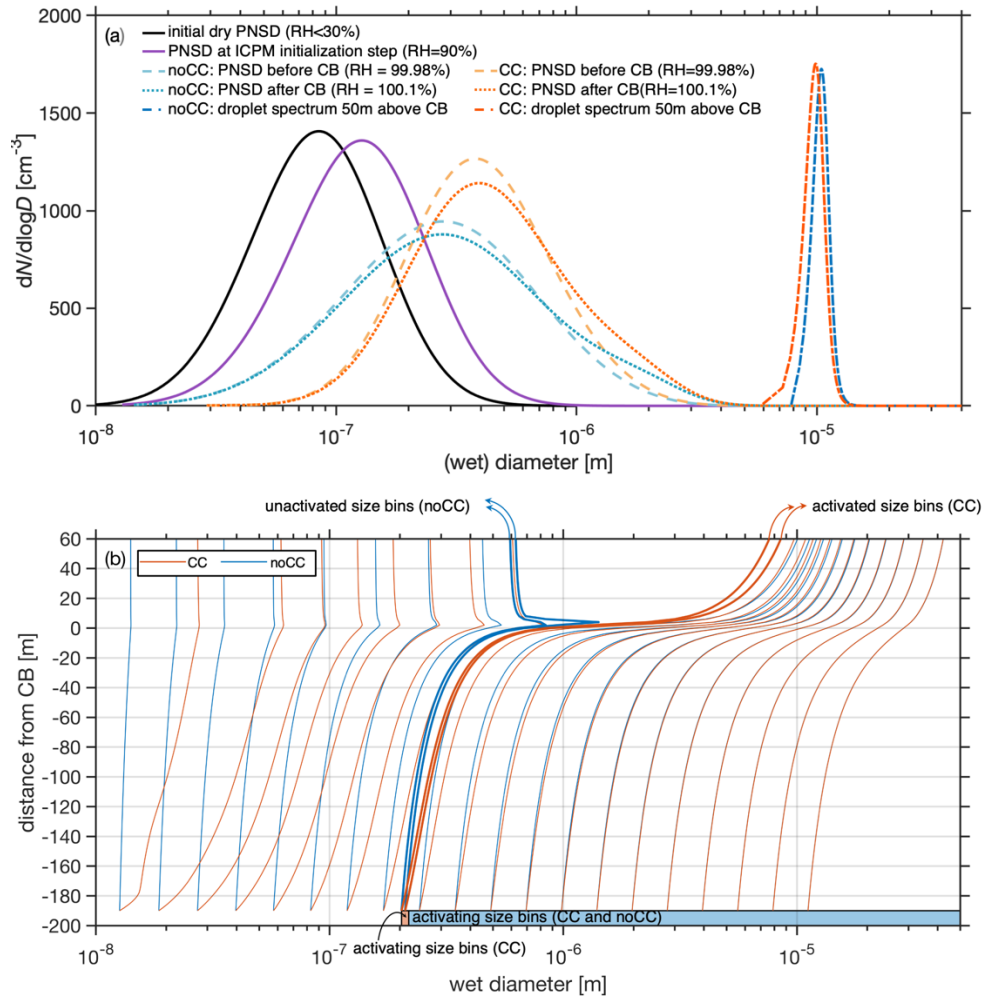
13  
14 *Correspondence to:* Liine Heikkinen (liine.heikkinen@aces.su.se) and Ilona Riipinen (ilona.riipinen@aces.su.se)

15  
16  
17 **Supplementary figures**



19  
20 **Figure S.1** A comparison between the FIGAERO-I-CIMS particle phase (sum of signals of identified ions in the particle  
21 phase) and the OA concentration measured with the ACSM. The data shown here are daytime values only (hour of day >9  
22 and <19) during the BA ECC campaign.

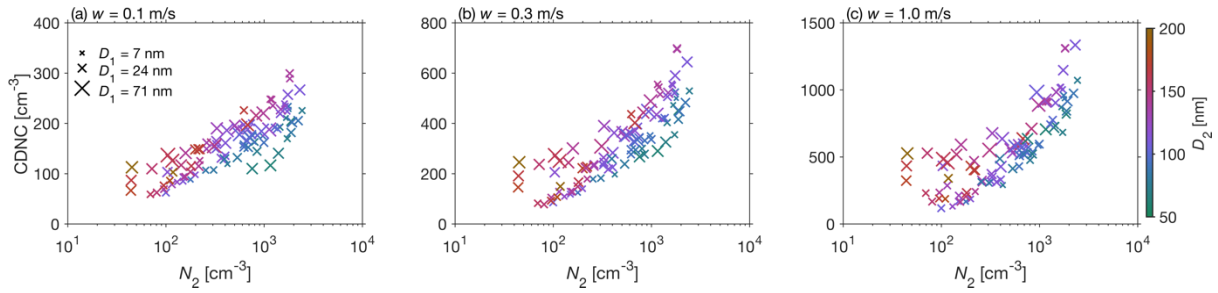
23



24

25 **Figure S.2 (a)** The evolution of the particle number size distribution (PNSD) during the May 11<sup>th</sup> case is shown in **Fig. 3**. The  
 26 size distributions are obtained from the simulations using a  $0.1 \text{ m s}^{-1}$  updraft velocity. Red lines correspond to simulations with  
 27 co-condensation (CC; F volatility distribution) and blue lines simulations without co-condensation (noCC). **(b)** The evolution  
 28 of the parcel model bin sizes (wet diameter; x-axis) as a function of altitude with respect to cloud base (CB; y-axis). The data  
 29 shown correspond to the simulation shown in panel **(a)**. The bin sizes grow below the cloud base more in the co-condensation  
 30 simulations which makes the red and blue lines drift as a function of altitude. The bolded curves show the evolution of size  
 31 bins corresponding to the range from the smallest activated dry radii with CC ( $r_{CC}^*=66.0 \text{ nm}$ ) to that modeled when CC is  
 32 turned off ( $r_{noCC}^*=71.9 \text{ nm}$ ). In this range size bins activate only when CC is turned on (red shaded area). This results in  
 33 activation of 4 more size bins as opposed to simulations where CC is turned off. Within the blue shaded area, all size bins  
 34 activate. The figure composes every 20<sup>th</sup> size bin out of the 400 bins included in the simulations. Within the red shaded size  
 35 range, every 2<sup>nd</sup> bin is displayed with bolded lines.

36  
 37



39

40 **Figure S.3** The relationship between cloud droplet number concentration (CDNC; y-axis) and accumulation mode number  
 41 concentration ( $N_2$ ; x-axis), accumulation mode geometric mean diameter ( $D_2$ ; color-coding), and Aitken mode geometric mean  
 42 diameter ( $D_1$ ; marker size) for the 0.1, 0.3 and 1.0 m s<sup>-1</sup> updraft scenarios, respectively (panels a–c) during BAECC. The  
 43 CDNC is obtained from simulations without co-condensation (noCC).  $N_2$ ,  $D_2$ , and  $D_1$  are used as model input data and represent  
 44 the bimodal fits performed on the measured PNSD using the fitting algorithm by Hussein et al. (2005).

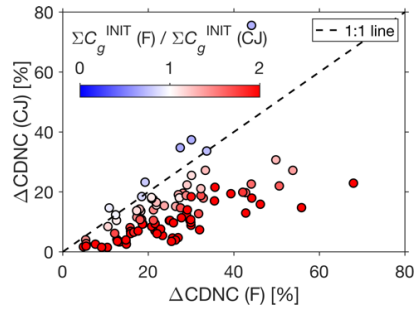
45

46

47

48

49



50

51 **Figure S.4** The relationship between CDNC enhancements due to co-condensation ( $\Delta$ CDNC) when F volatility distribution is  
 52 utilized (x-axis) vs when CJ distribution is utilized (y-axis). The markers from every 97 simulations are color-coded with the  
 53 initial concentration of organic vapor ( $\Sigma C_g^{\text{INIT}}$ ) in both simulation sets. The majority of the markers are red indicating that there  
 54 is more vapor present at the initial step of the ascent in simulations using the F volatility distribution. These red lines drift from  
 55 the 1:1 agreement predicting higher  $\Delta$ CDNC for the F simulations as opposed to CJ. When the difference in  $\Sigma C_g^{\text{INIT}}$  between F  
 56 and CJ simulations is negligible (white markers) also  $\Delta$ CDNC agree.

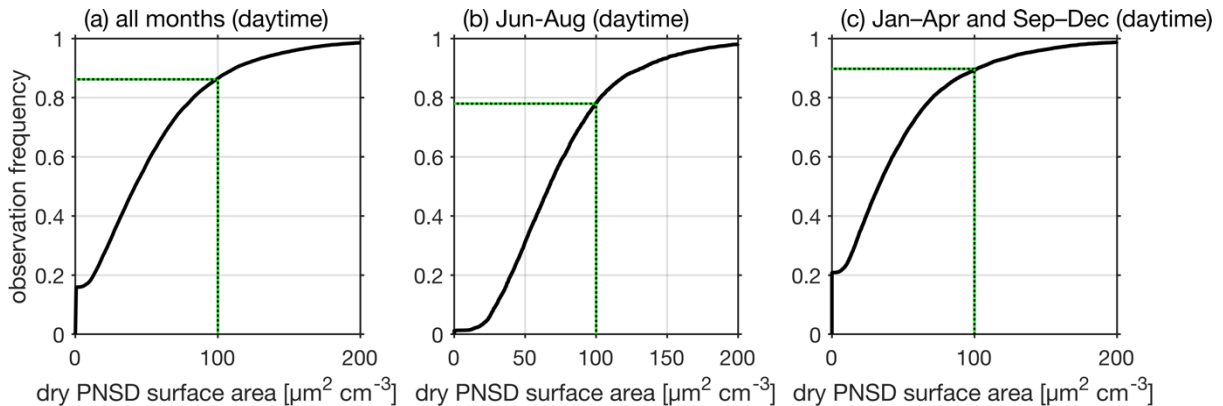
57

58

59

60

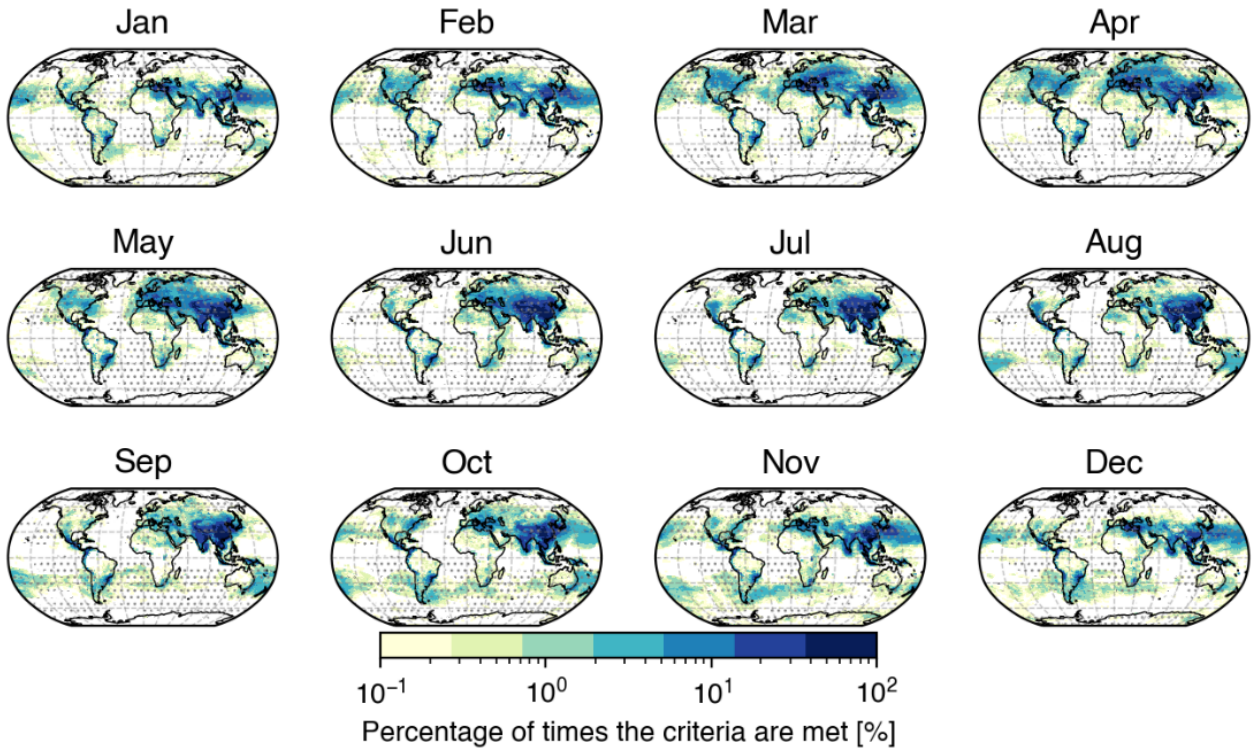
61



62

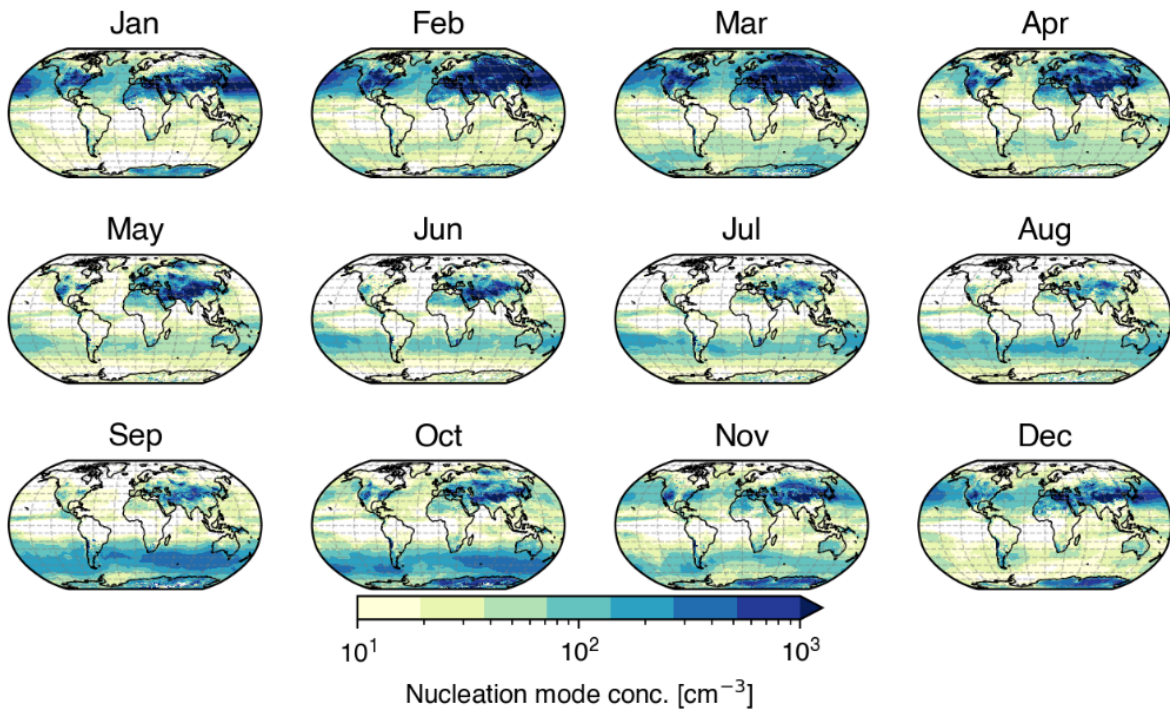
63

64 **Figure S.5** Cumulative density functions of the dry PNSD surface area calculated from the 2012–2017 SMEAR II DMPS data.  
 65 Panel a contains all the data, panel b the summer months and panel c the months outside summer. The green lines depict the  
 66 100  $\mu\text{m}^2 \text{cm}^{-3}$  threshold and the frequencies to which the calculated surface areas remain higher (86% of the time in panel a,  
 67 78% of the time in panel b and 90% of the time for panel c).



68  
69  
70  
71  
72  
73  
74  
75  
76  
77

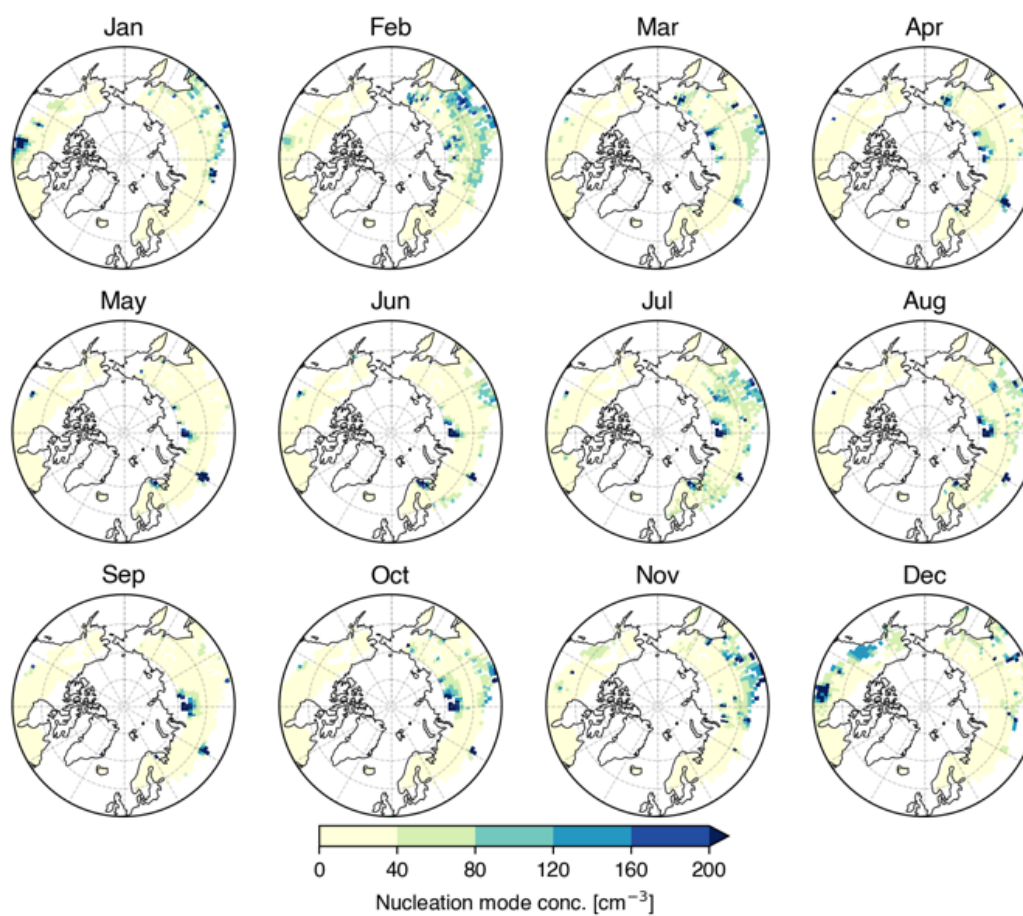
**Figure S.6** A global picture of the percentage of times the criteria are met in a 2009–2013 UKESM1 simulation.  $D_2$ ,  $D_1$  and  $N_1$  are the modal parameters representing the accumulation mode and Aitken mode parameters. The gray markers refer to boreal grid cells, where the median updraft velocity at cloud base is between  $0.2$  and  $0.5$   $\text{m s}^{-1}$ . Note the logarithmic axis of the color scale.



78  
79  
80

**Figure S.7** A global picture of the average daytime concentrations of the nucleation mode in the 2009–2013 UKESM1 simulation. Note the logarithmic axis of the color scale.

81  
82



83  
84  
85  
86  
87  
88

**Figure S.8** The average daytime concentrations of the nucleation mode in the 2009–2013 UKESM1 simulation. Only boreal grid cells are shown.